Combustion and Flame 198 (2018) 466–476

Contents lists available at ScienceDirect

Combustion and Flame

journal homepage: www.elsevier.com/locate/combustflame

A Physics-based approach to modeling real-fuel combustion chemistry – III. Reaction kinetic model of JP10

Yujie Tao[a], Rui Xu[a], Kun Wang[a], Jiankun Shao[a], Sarah E. Johnson[a], Ashkan Movaghar[b], Xu Han[c], Ji-Woong Park[d], Tianfeng Lu[d], Kenneth Brezinsky[c], Fokion N. Egolfopoulos[b], David F. Davidson[a], Ronald K. Hanson[a], Craig T. Bowman[a], Hai Wang[a,*]

[a] Department of Mechanical Engineering, Stanford University, Stanford, CA 94305-3032, USA
[b] Department of Aerospace and Mechanical Engineering, University of Southern California, Los Angeles, CA 90089-1453, USA
[c] Department of Mechanical and Industrial Engineering, University of Illinois at Chicago, Chicago, IL 60607-7042, USA
[d] Department of Mechanical Engineering, University of Connecticut, Storrs, CT 06269-3139, USA

ARTICLE INFO

Article history:
Received 2 May 2018
Revised 18 June 2018
Accepted 30 August 2018
Available online 18 September 2018

Keywords:
Kinetics
JP10
Reaction model
HyChem

ABSTRACT

The Hybrid Chemistry (HyChem) approach has been proposed previously for combustion chemistry modeling of real, liquid fuels of a distillate origin. In this work, the applicability of the HyChem approach is tested for single-component fuels using JP10 as the model fuel. The method remains the same: an experimentally constrained, lumped single-fuel model describing the kinetics of fuel pyrolysis is combined with a detailed foundational fuel chemistry model. Due to the multi-ring molecular structure of JP10, the pyrolysis products were found to be somewhat different from those of conventional jet fuels. The lumped reactions were therefore modified to accommodate the fuel-specific pyrolysis products. The resulting model shows generally good agreement with experimental data, which suggests that the HyChem approach is also applicable for developing combustion reaction kinetic models for single-component fuels.

1. Introduction

A Hybrid Chemistry (HyChem) approach has been recently proposed for high-temperature combustion chemistry modeling of multicomponent distillate fuels [1,2]. The fundamental premise of the approach is that in high-temperature fuel combustion, the pyrolysis or oxidative pyrolysis of the fuel is fast and precedes the oxidation of the pyrolysis products. As the key pyrolysis products are few and much less diverse in composition than the initial multicomponent fuel, these products can be followed kinetically in existing combustion kinetic experiments in shock tubes and flow reactors. The HyChem approach thus combines experimentally constrained, lumped reaction steps for fuel pyrolysis with a foundational fuel (C_{0-4} species plus benzene and toluene) chemistry model to describe the overall kinetic rate process of distillate fuel combustion. As a physics-based approach, HyChem seeks to establish the key relationship between cause and effect: the combustion chemistry properties of a real distillate fuel are governed more directly by the composition of its primary pyrolysis products than details of the initial fuel composition, as these details are washed out due to the principle of large component number in multicomponent fuel combustion [1,3].

Previously, we reported the application of the HyChem approach to three jet fuels and two rocket fuels [2]. These are all distillate fuels, each having complex composition. The purpose of the present work is to examine the applicability of HyChem to single-component fuels. For this purpose, we choose JP10 as the target fuel. JP10 is practically a single-component fuel, with chemically synthesized exo-tetrahydrodicyclopentadiene being over 96% weight fraction. With a lower heating value about the same as the conventional jet fuels (~43 MJ/kg), its volumetric energy density is significantly higher due to its high mass density of 0.940 kg/L at 15°C. With a basket-shaped, multi-ring structure, JP10 decomposes to a set of pyrolysis products that can be quite different from those of conventional jet fuels.

The reaction mechanisms of JP10 combustion have been studied at both detailed and lumped levels [4–8]. Notably, Gao et al. [7] proposed a detailed reaction model of 15518 reactions and 691 species and tested the model against a range of high-temperature pyrolysis and oxidation data of JP10, including speciation data from JP10 pyrolysis in a single-pulse shock tube and a flow tube reactor, and shock tube ignition delay. The semi-detailed model of Li et al. [5], on the other hand, uses only 27 reactions to describe

* Corresponding author.
E-mail address: haiwang@stanford.edu (H. Wang).

https://doi.org/10.1016/j.combustflame.2018.08.022
0010-2180/

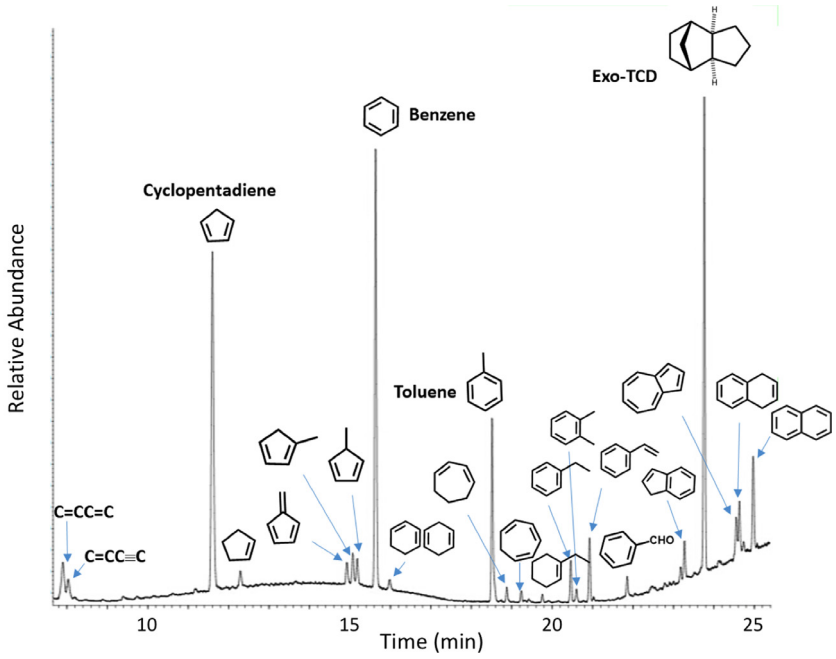

Fig. 1. Heavy species identified by GC-MS from oxidative pyrolysis of JP10 ($\phi = 1.0$, 450 ppm fuel input) in flow reactor at a reaction time of 28 ms, pressure of 1 atm and nominal temperature of 1137 K.

JP10 pyrolysis/oxidative pyrolysis on the basis of analogous decane and heptane chemistry and a detailed reaction model for $C_{0\text{-}3}$ compounds. It was shown that the model is capable of capturing global combustion properties, including the ignition delay [5] and non-premixed flame extinction and structures [9], rather well. The current work may be viewed as an extension of Li et al. [5], but in a HyChem context. Specifically, the selection of the intermediate pyrolysis products is guided by experiments to ensure all key species are considered in the model. Furthermore, the stoichiometric coefficients of the lumped reactions and their kinetic rates are subject to optimization using the Method of Uncertainty Quantification by Polynomial Chaos Expansions (MUM-PCE) [10–12], thus illustrating the efficiency and accuracy of the combined HyChem/MUM-PCE approach.

2. Experimental methods

Experiments were carried out for HyChem model parameter derivation and model testing. A brief overview is provided here, while a more detailed description can be found elsewhere [2].

2.1. Stanford shock tube facilities

Ignition delay time (τ_{ign}) and speciation experiments were carried out using both the high-pressure shock tube (HPST, 5.0 cm ID) and the low-pressure kinetics shock tube (KST, 14.1 cm ID) at Stanford University [13]. Ignition delay time was defined as the time interval between the arrival of the reflected shock at the observation port and the onset of ignition determined by extrapolating the maximum slope of the pressure or OH^* emission signals back to the baseline value; both methods yielded effectively the same ignition delay values. Speciation measurements in the HPST were made using a two-wavelength differential laser absorption method [14]. 10.532 μm and 10.675 μm were used to measure C_2H_4 and 3.17580 μm and 3.17595 μm were used to measure CH_4. In the KST experiments, a matrix method was used to simultaneously extract C_2H_4 and cyclopentadiene (C_5H_6) species time-histories from laser absorbance measurements at two wavelengths. The absorbance at 10.532 μm was dominated by C_2H_4, while the absorbance at 11.345 μm was dominated by C_5H_6. With minimal interference from other species (JP10, CH_4, C_3H_6, C_4H_8 isomers, C_5H_8, C_6H_6, and C_7H_8) at these two wavelengths, the two species time histories could be determined reliably from these two absorbance traces.

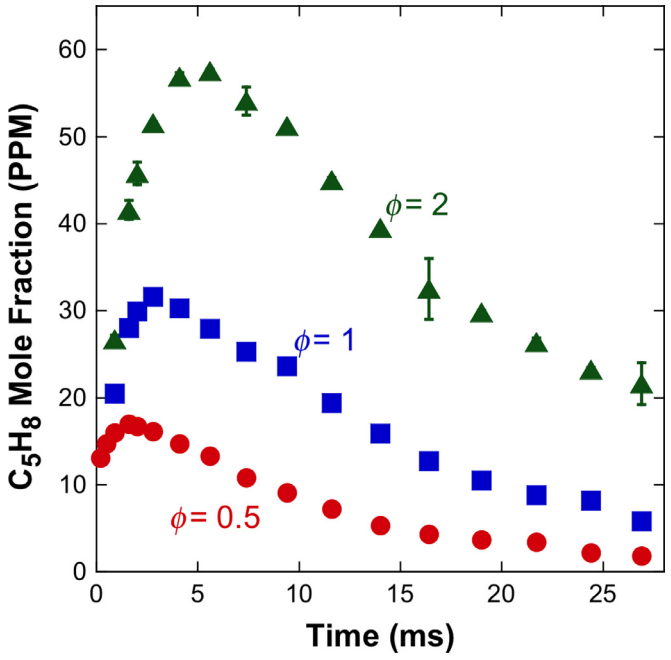

Fig. 2. Measured C_5H_8 time histories of JP10 oxidative pyrolysis in flow reactor under conditions specified in Table 1 ($p = 1$ atm). Error bars represent the uncertainty due to data scatter.

2.2. UIC shock tube facilities

The low-pressure, heated, single pulse shock tube (6.35 cm ID in the driven section) [15,16] was used for pyrolysis speciation. The

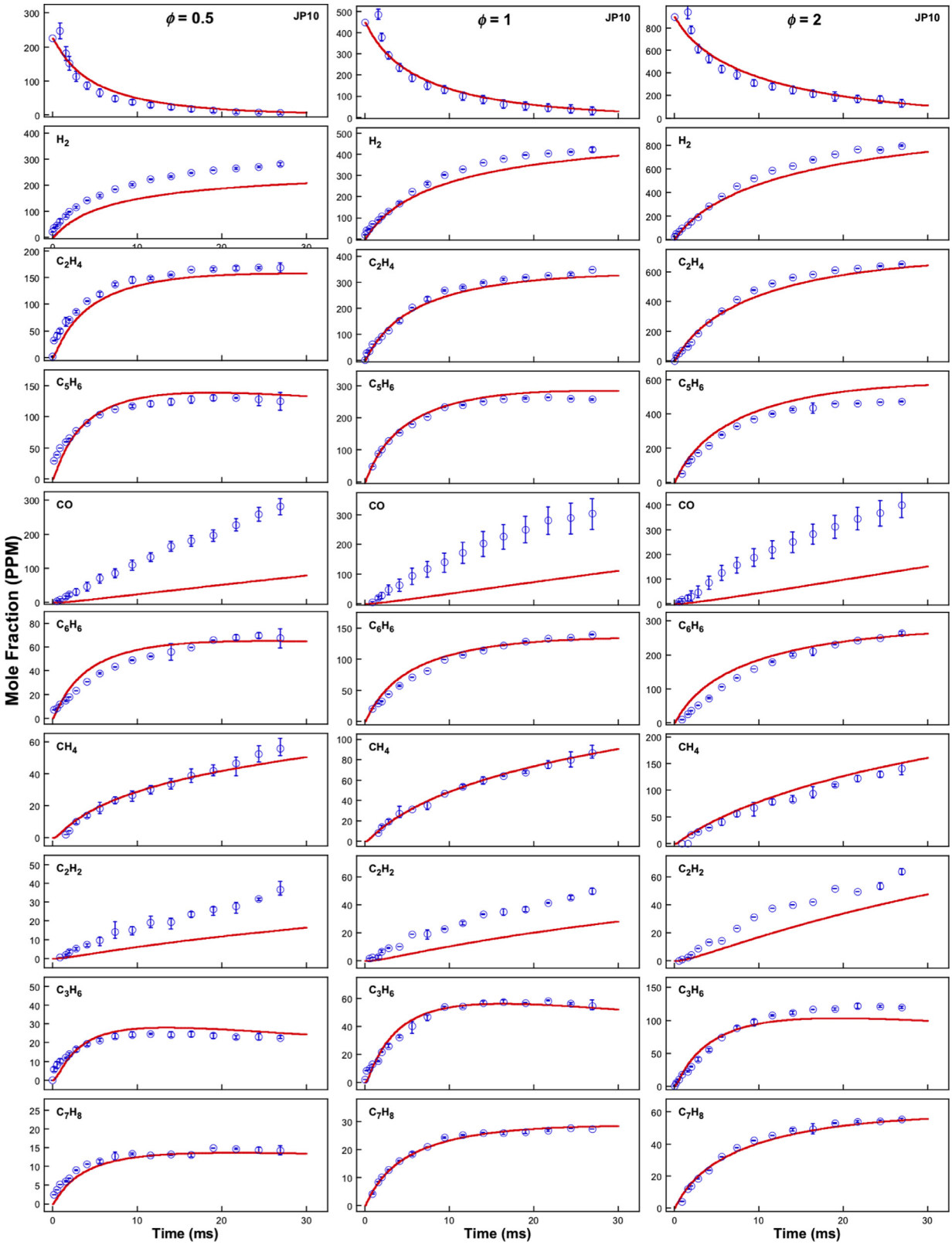

Fig. 3. Experimental (symbols) and simulated (lines) key species during the oxidative pyrolysis of JP10 in a flow reactor at three equivalence ratios. See Table 1 for experimental conditions.

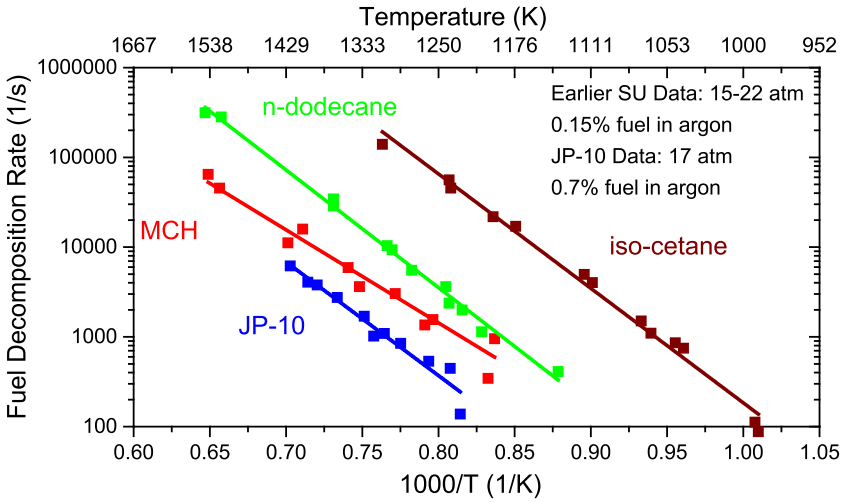

Fig. 4. Fuel decomposition rate observed for JP10 (this work) compared with *n*-dodecane, *iso*-cetane and methyl-cyclohexane (MCH) reported in [35]. Symbols are experimental data, lines are fits to data.

reaction time is measured as the time lapse from the shock arrival to when the pressure is 80% of its maximum value [16]. The reacted gas was sampled from the end wall by gas chromatography (GC) with an flame ionization detector. The initial JP10 concentration in the reactant mixture is determined in calibration experiments in which the CO_2 measured from a full fuel oxidation (under fuel lean condition) is equated to the JP10 concentration on a carbon basis. The carbon balance for the experiments reported herein is better than 90%.

2.3. Flow reactor facility

The flow reactor [17] experiment is conducted at ambient pressure. The fuel vapor-nitrogen mixture is injected into the products of a H_2/air flame stabilized on a water-cooled McKenna burner to provide a hot vitiated flow into the reactor tube. To ensure that the reaction takes place under near adiabatic conditions, the quartz reactor tube is electrically heated by temperature-controlled heaters. The reaction products are sampled by a cooled extraction probe and are sent to a 4-column micro GC (Inficon microGC 3000) and a GC-MS (mass spectrometer, Agilent 7890 GC with 5977 MSD) that provides real-time detection. A non-dispersive infrared analyzer and a paramagnetic analyzer were used for real-time measurements of CO, CO_2 and O_2 for comparison with the GC measurements. The total uncertainty in species concentration is ±2–5% for most species. The carbon balance is better than 95%.

2.4. Laminar flame speeds and extinction strain rates

Laminar flame speed, S_u°, was measured in the counterflow configuration for a wide range of equivalence ratios at atmospheric pressure and an unburned mixture temperature $T_u = 403$ K. A double pulsed ND:YAG laser and a high performance 12 bit CCD camera with 1376×1040 pixels of resolution was used to acquire particle image velocimetry images. The minimum axial velocity along the system centerline just upstream of the flame is defined as a reference flame speed, $S_{u,\mathrm{ref}}$, and the maximum absolute value of axial velocity gradient is defined as a local strain rate, K. As K is varied, its effect on $S_{u,\mathrm{ref}}$ is recorded, and S_u° is determined through computationally-assisted extrapolation to zero stretch [18].

High-pressure S_u°'s were measured in the constant volume spherical expanding flame configuration [19]. The stainless-steel chamber has an internal diameter of 203.2 mm and can withstand pressure up to 200 atm. The flame speed is determined from the pressure time history using the direct numerical method and hybrid thermodynamic-radiation model [19].

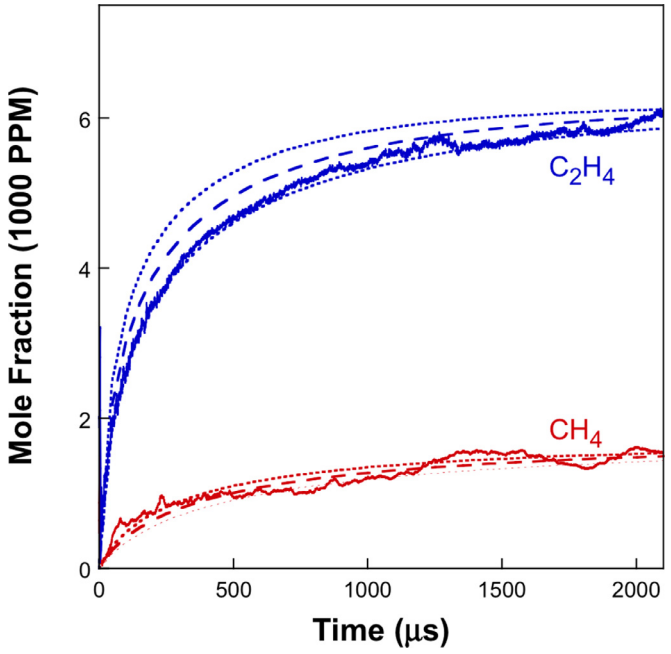

Fig. 5. Time histories of C_2H_4 and CH_4 measured (solid lines) and simulated (dashed lines) during 0.72 %(mol) JP10 pyrolysis in Ar at $T_5 = 1363$ K and $p_5 = 17.2$ atm. The dotted lines are simulations bracketing the ±15 K temperature uncertainty.

Extinction strain rates, K_{ext}, were measured in the counterflow configuration at atmospheric pressure for non-premixed flames by impinging a fuel/N_2 stream at $T_u = 473$ K onto an ambient temperature O_2 stream. In order to determine the K_{ext}, a near-extinction flame is established, and then the strain rate K is measured on the fuel side and extinction is achieved by reducing slightly the fuel concentration.

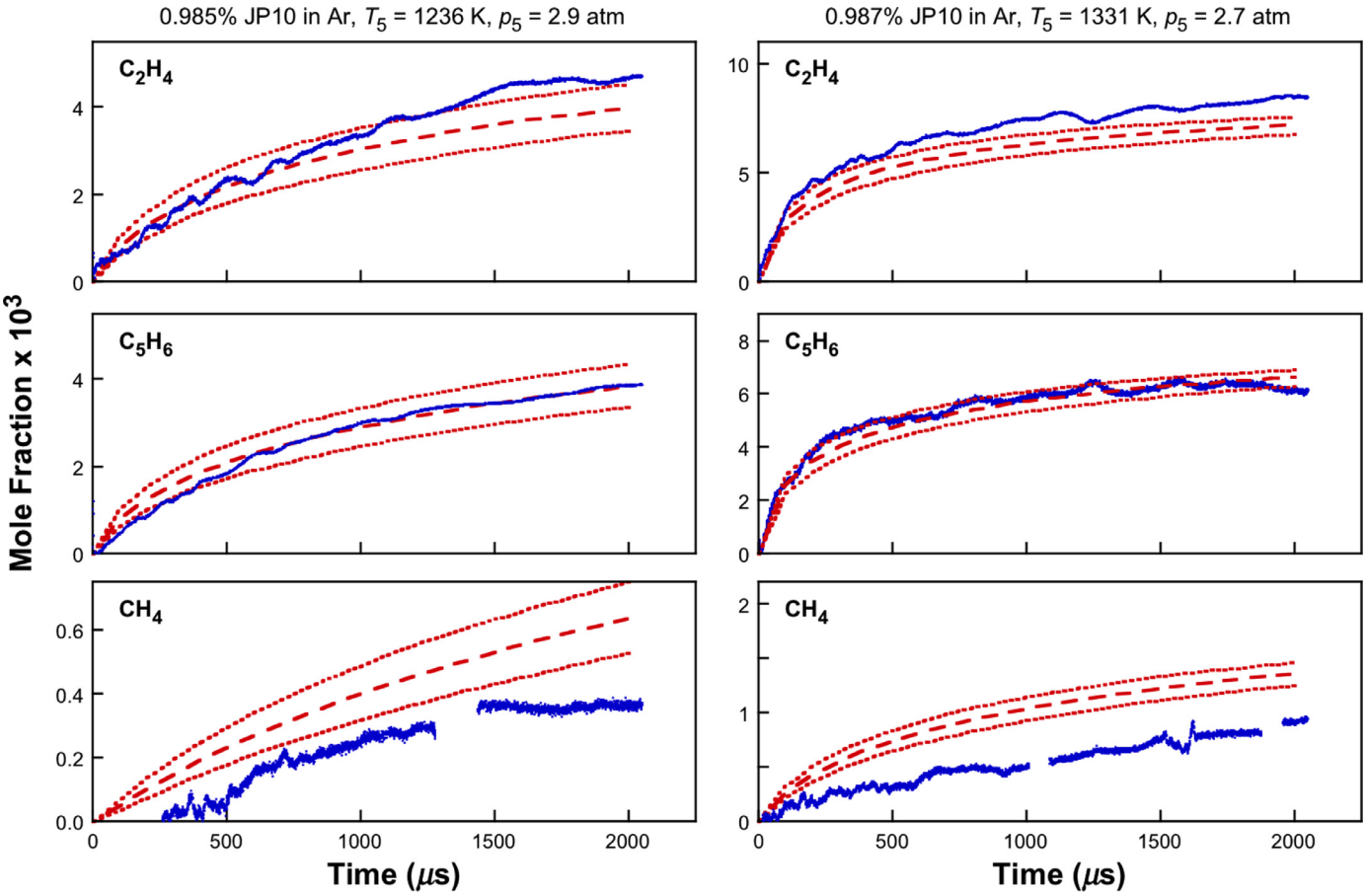

Fig. 6. Selected time histories of C_2H_4, C_5H_6 and CH_4 measured and simulated (dashed lines) during JP10 pyrolysis in Ar. The dotted lines are simulations bracketing the ±15 K temperature uncertainty.

3. The HyChem model and its development

As described earlier, the HyChem approach [1,2] combines a lumped, experimentally constrained pyrolysis model with a detailed foundational fuel chemistry model to describe the oxidation of the pyrolysis intermediates, which is currently USC Mech II [20], which includes the high-temperature combustion reactions for H_2, CO, $C_{1\text{-}4}$ hydrocarbons, cyclopentadiene, benzene and toluene.

Thermochemical data of JP10 were taken from the Third Millennium Ideal Gas and Condensed Phase Thermochemical Database [21]. Transport properties of the JP10 molecule were estimated using the method of corresponding states [22]. Because the high-pressure flame speeds were measured with diluent gases N_2 and He, the accuracy of the He-N_2 binary diffusion coefficient is critical to a reliable prediction of the experiment. As reported in [23], the repulsive part of the Lennard–Jones (L-J) 12-6 potential function is too stiff to accurately model diffusion coefficients at high temperatures. The binary diffusivity coefficient D and collision integral ratios A^*, B^*, and C^* of He-N_2 were calculated using the potential energy surface measured from a molecular beam experiment [24]. The four quantities were then parameterized in the same way as described in [25] and read directly into a modified version of Tranfit [26] with an updated transport library and interpreter. The parameter values are available as a part of the transport data file in the web release of the reaction model at http://web.stanford.edu/group/haiwanglab/HyChem/Index.html.

Earlier, we presented evidence that for jet and rocket fuels, only a small number of pyrolysis intermediates are important to model the heat release in laminar premixed flames and induction period radical build up during fuel ignition [1,2]. For the single component JP10, we find this to be the same, as will be shown later. Major decomposition products are cyclopentadiene (C_5H_6), benzene (C_6H_6), and toluene (C_7H_8) in addition to ethylene (C_2H_4) and propene (C_3H_6).

The lumped fuel decomposition reactions are expressed in a way that allow for stoichiometric coefficient estimation based on experimental data:

$$C_{10}H_{16} \rightarrow e_a(C_2H_4 + \lambda_3 C_3H_6 + \lambda_5 C_5H_6 + \lambda_0 H_2) + b_d[\chi C_6H_6 + (1-\chi)C_7H_8] + \alpha H + \gamma a C_3H_5 + (2-\alpha-\gamma)CH_3 \quad \text{(R1)}$$

$$C_{10}H_{16} + R \rightarrow RH + e_a(C_2H_4 + \lambda_3 C_3H_6 + \lambda_5 C_5H_6 + \lambda_0 H_2) + b_a[\chi C_6H_6 + (1-\chi)C_7H_8] + \beta H + \theta a C_3H_5 + (1-\beta-\theta)CH_3 \quad \text{(R2)}$$

where aC_3H_5 is the allyl radical which is considered here because of the decomposition pathways unique to the parent fuel molecule. Reaction (R1) represents the C–C fission in the fuel molecule, followed by the decomposition of the resulting radical fragments. Reaction (R2) describes the H-abstraction by radical R followed by β-scission of the resulting fuel radical. We consider R to be H and CH_3 for pyrolysis, and O, OH, O_2 and HO_2 with oxidation in addition. In (R1) and (R2), e_d, e_a, b_d and b_a are dependent stoichiometric coefficients which may be determined from the dependent coefficients λ_3, λ_5, λ_0, χ, α, β, γ, and θ by atom balances:

$$\text{Carbon (R1)}: \ 10 = e_d(2 + 3\lambda_3 + 5\lambda_d) + b_d(7-\chi) + 2 - \alpha + 2\gamma \quad (1)$$

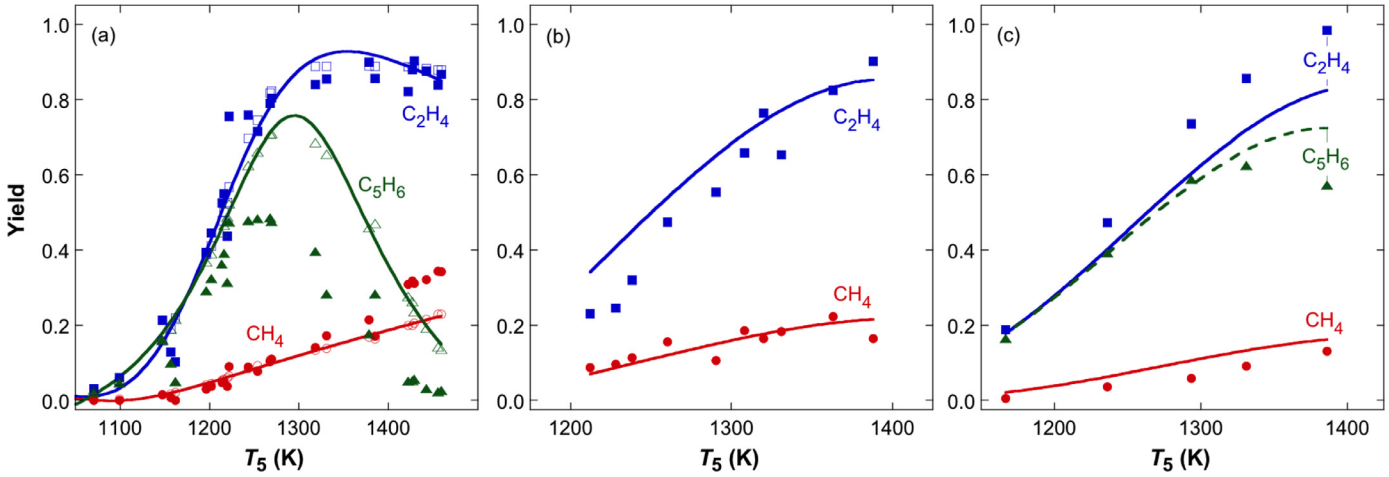

Fig. 7. Experimental (solid symbols) and simulated (open symbols and lines) yields of CH_4, C_2H_4, and C_5H_6 at a nominal reaction time of 2 ms from JP10 pyrolysis in (a) UIC shock tube (75 PPM JP10 in Ar, $p_5 = 12$ atm), (b) Stanford high pressure shock tube (6900 PPM JP10 in Ar, $p_5 = 17$ atm) and (c) Stanford kinetic shock tube (1 mol% JP10 in Ar, $p_5 = 3$ atm). In modeling the UIC shock tube experiments, reaction times measured individually for each experiment are used for the respective simulation. The lines are fits to the corresponding modeled quantities.

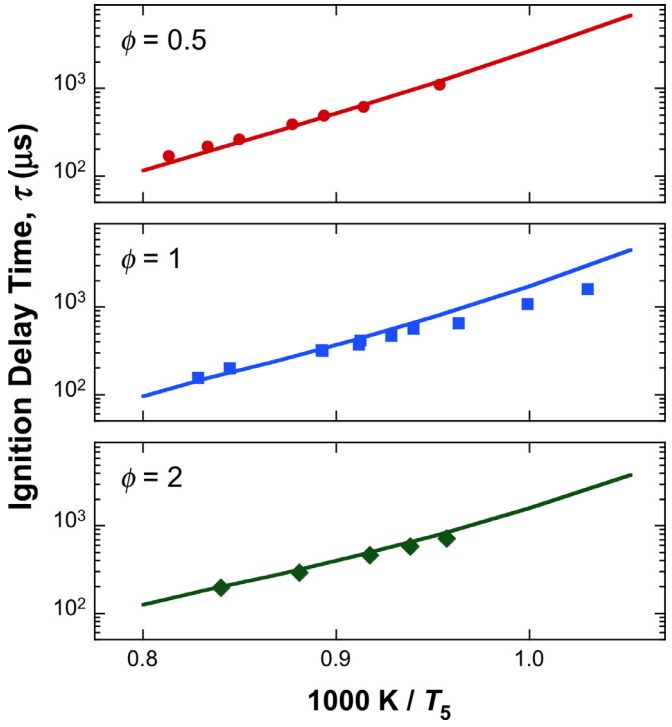

Fig. 8. Experimental (symbols, this work) and simulated shock tube ignition delay of JP10 in air at 17 atm.

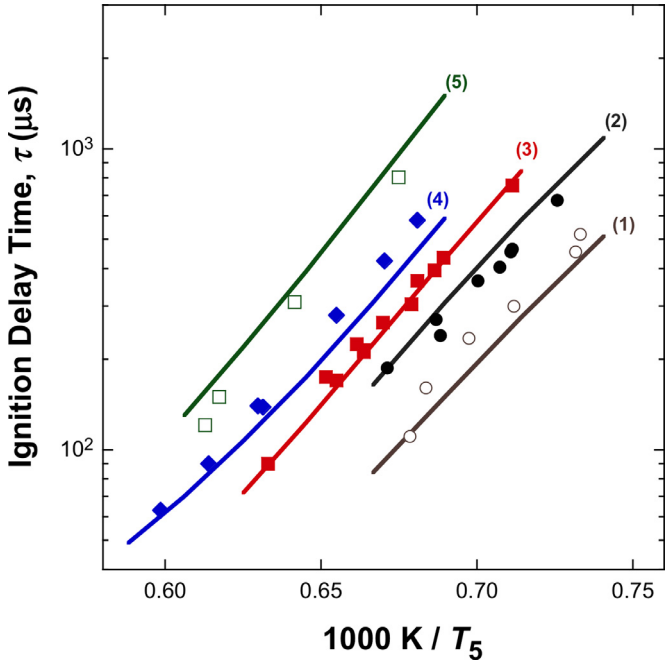

Fig. 9. Experimental (symbols, taken from [29]) and simulated (lines) shock tube ignition delay of 0.2 mol% JP10 in O_2 and Ar at several pressures and equivalence ratios: (1) $p_5 = 3$ atm, $\phi = 0.5$; (2) $p_5 = 6$ atm, $\phi = 1$; (3) $p_5 = 3$ atm, $\phi = 1$; (4) $p_5 = 1$ atm, $\phi = 1$; (5) $p_5 = 3$ atm, $\phi = 2$.

$$\text{Hydrogen (R1)}: 16 = 2e_d(2 + 3\lambda_3 + 3\lambda_d + \lambda_0) + b_d(8 - 2\chi) + 6 - 2\alpha + 2\gamma \quad (2)$$

$$\text{Carbon (R2)}: 10 = e_a(2 + 3\lambda_3 + 5\lambda_d) + b_a(7 - \chi) + 1 - \beta + 2\theta \quad (3)$$

$$\text{Hydrogen (R1)}: 15 = 2e_a(2 + 3\lambda_3 + 3\lambda_d + \lambda_0) + b_a(8 - 2\chi) + 3 - 2\beta + 2\theta \quad (4)$$

The physical significance of the independent stoichiometric coefficients is self-explanatory. α and β are the numbers of H radicals generated in R1 and R2, respectively; γ and θ are the numbers of aC_3H_5 radicals. Since the total numbers of radicals generated are two and one for (R1) and (R2), respectively, the number of methyl (CH_3) radicals are $2 - \alpha - \gamma$ and $1 - \beta - \theta$, respectively. The coefficients λ_3, λ_5, and λ_0 are the C_3H_6-, C_5H_6-, and H_2-to-C_2H_4 ratios, and χ is the fraction of C_6H_6 in the total aromatics comprised of benzene and toluene. With USC Mech II as the foundational fuel chemistry model, the entire reaction model is comprised of 120 species and 841 reactions.

Rate coefficients were first estimated from analogous reactions, and they were then tuned against experimental data by systematic optimization. The initial rate coefficient of the C–C fission reaction

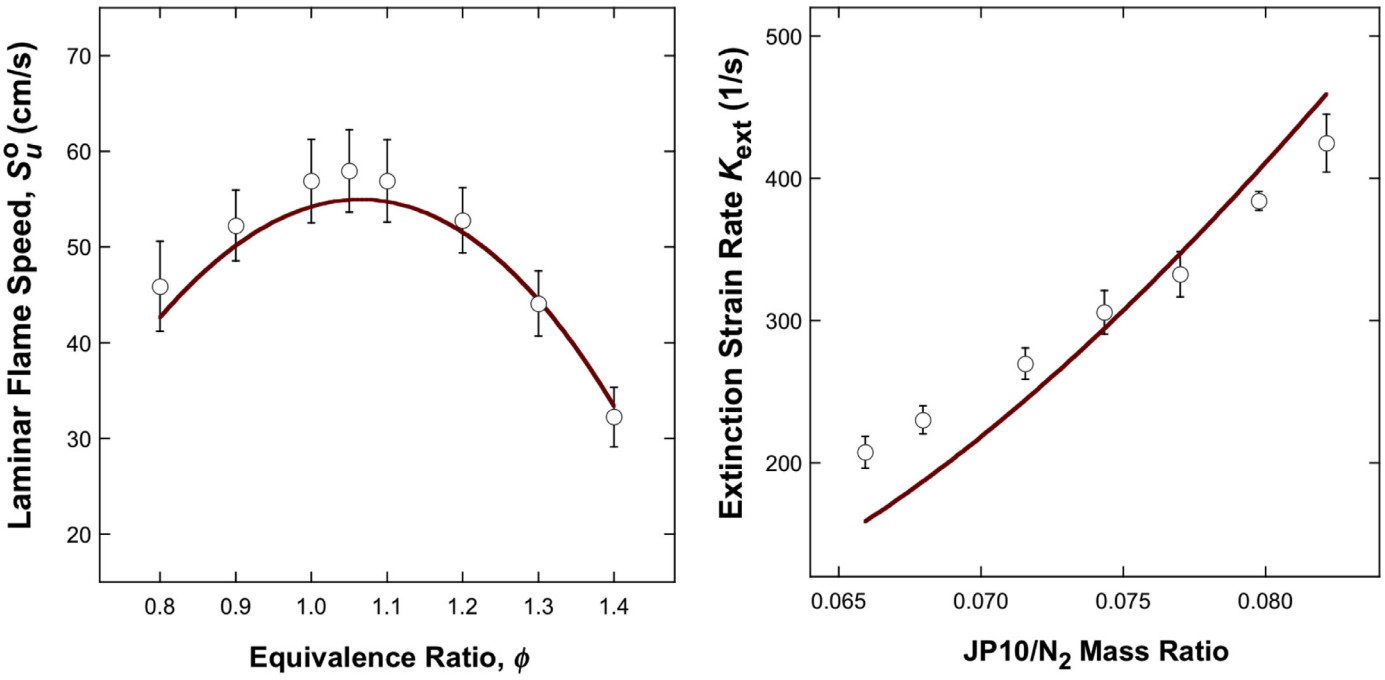

Fig. 10. Experimental (symbols) and simulated (lines) laminar flame speed of JP10-air mixture at 1 atm pressure and 403 K unburned gas temperature (left panel) and extinction strain rate of non-premixed JP10/N_2 against O_2 (1 atm pressure, and the JP10/N_2 jet temperature at 473 K and the O_2 jet temperature at 300 K) (right panel). The error bars represent $\pm 2\sigma$ data uncertainties.

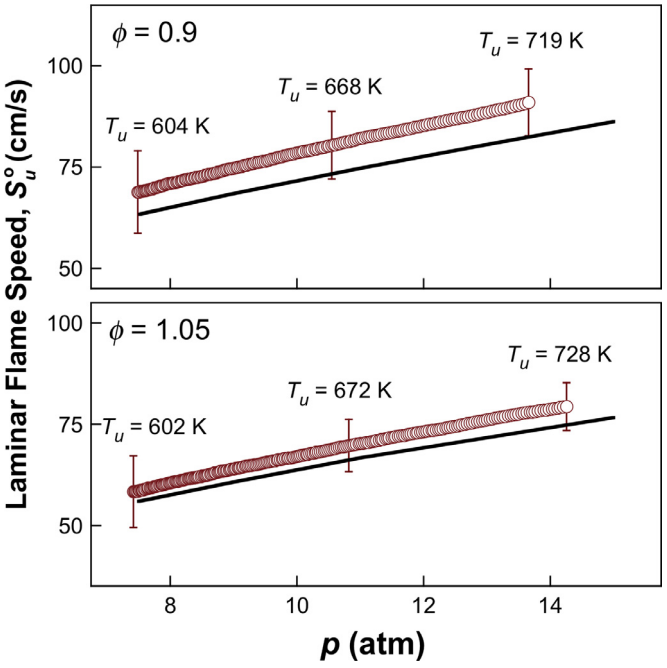

Fig. 11. Experimental (symbols) and simulated (lines) laminar flame speed of JP10 in O_2 diluted by N_2 and He at the equivalence ratio of 0.9 (top panel: 0.9 JP10/14 O_2/51.75 He/34.5 N_2) and 1.05 (bottom panel: 1.05 JP10/14 O_2/57.75 He/38.5 N_2) at elevated pressures. The temperature values given in the plots are the unburned gas temperatures at the corresponding pressures. The error bars represent $\pm 2\sigma$ data uncertainties.

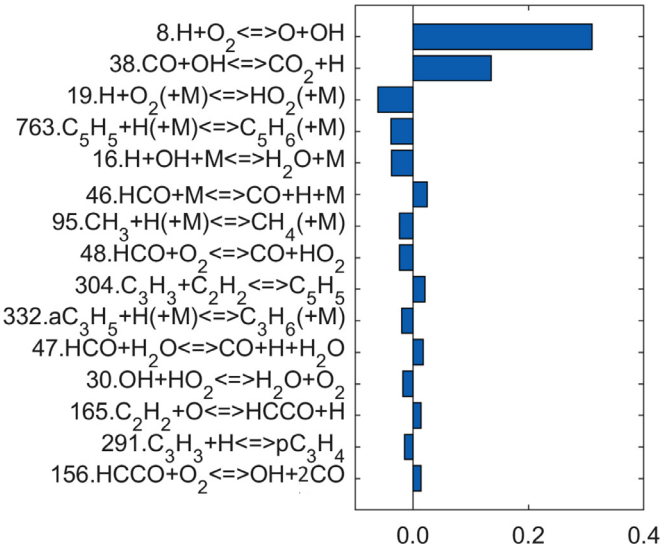

Fig. 12. Ranked sensitivity spectrum of laminar flame speed computed at $p = 13.7$ atm and $T_u = 719$ K.

(R1) was estimated from a measurement of the disappearance rate of JP10 [4]. The H-abstraction reaction rates were estimated from analogous reactions. Specifically, in each fuel molecule, there are 6 secondary carbons and 4 tertiary carbons. The rate coefficients for the secondary carbons are from those of cyclohexane and those of the tertiary carbon are from i-C_4H_{10}. The overall rate coefficients were estimated from

$$k = k_{c\text{-}C_6H_{12}+R\rightarrow RH+c\text{-}C_6H_{11}} + 4k_{i\text{-}C_4H_{10}+R\rightarrow RH+t\text{-}C_4H_9}$$

for R = H, CH_3 and O, and

$$k = k_{c\text{-}C_6H_{12}+R\rightarrow RH+c\text{-}C_6H_{11}} + \frac{4}{3}k_{i\text{-}C_4H_{10}+R\rightarrow RH+t\text{-}C_4H_9}$$

for R = OH, O_2 and HO_2 based on the symmetry numbers of the reactants and products [27]. The rate coefficients on the right hand side of the above equations were taken from JetSurF 2.0 [28]. Because the tentative rates are subject to further optimization, the estimates only provide a starting point for the HyChem rate coefficients. The 7 reaction rate coefficients, plus 8 independent stoichiometric parameters, give us a total of 15 parameters in the inverse problem.

In formulating (R1) and (R2), cyclopentene (C_5H_8) was not considered. As will be discussed later, cyclopentene is produced as an intermediate in a notable concentration, but it quickly decomposes to cyclopentadiene and other species with the range of temperature relevant to high-temperature combustion of JP10. Flow reactor experiments have shown that the carbon in cyclopentene never exceeded 4% of the total carbon, as will be shown later. Further, whether or not to include it as a product of reaction (R1) and (R2) does not noticeably impact the product distribution other than C_5H_8 itself.

Stoichiometric coefficients were initially estimated from the experimental yield ratios. They were subject to subsequent optimization along with the tentative set of rate parameters. The ranges were set to be narrow enough so that the response surface accuracy is satisfactory. A total of 180 targets were chosen for parameter optimization, among which 122 data points were retained after the consistency test [10], covering temperature from 1045 to 1671 K and pressure from 1 to 17 atm. The fact that many target data points were deemed inconsistent is not a serious concern because a fairly conservative approach was adopted for the consistency check [10]. The approach was designed not to let one or more data points to overly skew the optimized model parameters when the corresponding data uncertainty is under-estimated. Targets taken from flow reactor are: major and secondary species mole fraction at 4.1 ms and 21.7 ms. One standard deviation σ of flow reactor measurements was estimated to be 10% for major species and 15% for secondary species. For C_2H_4, CH_4 and C_5H_6 time-history profiles from the Stanford shock tube experiments, targets were selected as the mole fractions at 0.2 and 1.5 ms with σ taken to be 15%. For the rate of fuel disappearance, targets were defined as the fuel mole fraction at 0.5 ms of reaction time, with the same 15% σ value. Table S1 of the Supplementary Materials (SPM) lists all the targets retained in the optimization. In principle, the HyChem approach uses the measured pyrolysis species concentration for model parameter determination [1,2]. Unlike the earlier jet and rocket fuel work in which we used species time-history data from oxidative pyrolysis of a fuel in shock tube to constrain the rate coefficients of the H-abstraction reactions (R2) by O_2, HO_2 and OH, these data are unavailable here. For this reason, a total of 12 shock tube ignition delay time targets were included in the optimization. They were selected as the highest and lowest temperatures of each set of data of the present work and from Ref. [29]. The σ value of τ_{ign} were estimated to be 10%.

Model optimization component of the MUM-PCE approach [10] was used to obtain the optimized HyChem parameters. The trial parameters are assumed to have a uniform distribution within their respective bounds. The objective function is

$$\Phi(\mathbf{x}^*) = \min_{\mathbf{x}} \left\{ \sum_{r=1}^{M} \left(\frac{\eta_r^{\text{calc}}(\mathbf{x}) - \eta_r^{\text{expt}}}{\sigma_r^{\text{expt}}} \right)^2 \right\}$$

where $\mathbf{x}$ represents the normalized parameter array, M is the total number of targets, $\eta_r^{\text{calc}}(\mathbf{x})$ is model prediction with a given set of HyChem parameters, expressed as a response surface [30], η_r^{expt} is the experimental target value, and σ_r^{expt} its standard deviation. Kinetic modeling for solution mapping and model testing was carried out using the Sandia Chemkin package [26,31–33].

4. Results and discussion

4.1. Model development

We discuss first the key species identified in the oxidative pyrolysis experiments in the flow reactor at 1137 K. Among the heavy species detected at the end of the flow reactor corresponding to 28 ms of reaction time (Fig. 1), cyclopentadiene, benzene, toluene along with the unreacted fuel, are the four key species. Naphathalene was detected at a notable abundance, but it is not treated in the model. At the level detected (~10 ppm), naphathalene can hardly impact the main reaction chemistry, because its concentration is substantially lower than that of benzene at ~140 ppm under the same condition. Although cyclopentene is seen to have a small concentration at the end of reaction, its concentration can be rather significant during the early stage of reaction. As discussed earlier, cyclopentene could be included as a key pyrolysis species in reactions (R1) and (R2), but we decided to leave it out since its concentration decays rather faster at 1137 K, as shown in Fig. 2. Toward higher temperatures, the decay rate would be even faster. In any case, the carbon content in cyclopentene never exceeded 4% of the total carbon in all three equivalence ratios tested in the flow reactor.

Table 1
Temperature and initial mole fractions of the flow reactor experiments.

	$\phi = 0.5$	$\phi = 1$	$\phi = 2$
T (K)	1137	1135	1130
JP10	0.000225	0.000450	0.000900
CO_2	0.000228	0.000228	0.000228
Ar	0.00508	0.00508	0.00508
O_2	0.00626	0.00626	0.00626
H_2O	0.215	0.215	0.215
N_2	0.773	0.773	0.772

Table 2
Optimized stoichiometric parameters.

Parameter	Value	Parameter	Value
α	1.79	λ_0	0.53
γ	0.20	λ_3	0.02
β	0.24	λ_5	1.10
θ	0.48	χ	0.80

Given the wide ranges of the parameter values and considering that the accuracy of the response surface is critical to the optimization result, optimization was done in a piecewise, iterative fashion with updated parameter ranges and response surfaces for each step, until convergence on both the rate and stoichiometric parameters, and model results. Table 2 shows the values of the optimized stoichiometric parameters. The rate coefficients are given as a part of the reaction model release available at http://web.stanford.edu/group/haiwanglab/HyChem/Index.html.

Time history data of species from the oxidative pyrolysis of JP10 in the flow reactor are shown in Fig. 3, along with simulation results of the optimized HyChem model. Keeping in mind that the flow reactor used vitiated gas, the initial mixture contains a substantial amount of water vapor, as shown in Table 1. From our jet-fuel studies [2], we found that the presence of water primarily impacts methane production. It does not impact the distribution of other products. The initial rise-then-fall behavior of JP10 is due to the finite rate of mixing at the entrance of the flow reactor. Beyond the mixing region, the temperature is within ±1 K random error. The mean values were settled at 0, 2, and 7 K lower than the nominal, non-reacting temperature for ϕ = 0.5, 1, and 2 respectively. The temperature decrease is due to the endothermicity of fuel cracking. The experiment was modeled as a constant pressure, constant temperature process, with consideration of the respective temperature drops.

While the fuel is almost depleted after the total reaction time of 28 ms, the oxygen concentration only slightly lowered. For the ϕ = 1 mixture, 3% of total O_2 was consumed. In agreement with earlier studies [4,7,34], the decomposition intermediate that contains the greatest amount of carbon is cyclopentadiene, which

accounts for one quarter of the total carbon. This is different from conventional jet fuels, in which cyclopentadiene was negligible [2]. Benzene C_6H_6 and C_2H_4 are the next most abundant intermediates on a carbon basis.

Agreement is generally good between experiment and model across all three equivalence ratios. Exceptions are CO and C_2H_2, where the model predictions are significantly lower than the measurements. The difference between the measured and predicted CO at 28 ms, i.e., the end of the reaction time tested, amounts to a total of ~5% of the carbon for all three equivalence ratios. For CO, the discrepancy is attributable to missing channels that could directly form CO at the very early stage of reaction. In addition to the possible limitation of the HyChem assumption about fuel pyrolysis being fully decoupled from the oxidation of the decomposed products, another cause for the discrepancy is the incomplete C_5 and C_6 chemistry in USC Mech II, as discussed in Section S2 of the SPM, where the discrepancy of C_2H_2 is also discussed. Hence, no additional effort was made to improve the predictions for CO and C_2H_2. It is important to note that neither of the available JP10 models [5,7] predicts the time histories of CO and C_2H_2 well. Hence, further research in this area is needed.

Considering the high CO production, it is also possible that CO is not produced solely from the oxidation of the intermediate hydrocarbon species. This observation reveals a potential limitation of the HyChem approach—while fully decoupled fuel pyrolysis followed by the oxidation of the pyrolysis intermediates is one of the key HyChem assumptions, direct fuel oxidation and CO production can occur alongside fuel pyrolysis in some cases. Considering the low decomposition rate of JP10 measured in this study as compared to representative hydrocarbon components of jet fuels as shown in Fig. 4, JP10 could be an extreme case for testing the assumption of complete decoupling. It was observed in flow reactor oxidative pyrolysis experiments that to have a similar fuel consumption in 30 ms, the temperature in the JP10 experiment is ~100 K higher than those measured for other jet fuels. Nonetheless, the under-prediction of CO does not pose severe problem that would limit the ability of the model to predict global combustion properties, as will be discussed later.

Species profiles of CH_4, C_2H_4 and C_5H_6 during JP10 pyrolysis are shown in Figs. 5 and 6 in the Stanford HPST and KST shock tubes, respectively. The experimental and computed C_2H_4 and C_5H_6 time history profiles are in reasonably good agreement. Experimentally, CH_4 time histories are generally less smooth than the C_2H_4 data because the concentration of CH_4 is quite small. The trends are well captured by the model. The measurements of JP10 pyrolysis in the UIC low-pressure shock tube were not included in model optimization. Rather, the data are used for independent model test as shown in Fig. 7a. Also included in Fig. 7b and 7c are comparisons for the yields of CH_4, C_2H_4, and C_5H_6 at 17 and 3 atm for data collected in Stanford shock tube (panels b and c). It can be seen that the simulated species yields generally agree well with the experimental data. The only exception is the C_5H_6 measured in the UIC shock tube, as shown in Fig. 7a. We note that the model reproduces the C_5H_6 concentrations measured in the Stanford shock tube, and for this reason, the discrepancy is likely to be caused by experimental issues.

4.2. Tests against global combustion properties

Comparisons for the global combustion properties, including the shock tube ignition delay time (IDT), flame speed and non-premixed flame extinction strain rate are discussed next. Figure 8 shows the measurements from the Stanford HPST for JP10/air IDT at 17 atm, covering the temperature range from 971 to 1230 K. The overall agreement between the experiment and model is good, but the model prediction curves up at a higher slope than the experiment, especially for $\phi = 1$. This difference may be attributable to the low-temperature chemistry not considered in the current HyChem model, which may play a role under such condition. Figure 9 shows the comparison of model prediction of τ_{ign} against data reported in Ref. [29]. The data were taken at a higher temperature than those shown in Fig. 8 and with Ar as the diluent gas. Again, the agreement is acceptable.

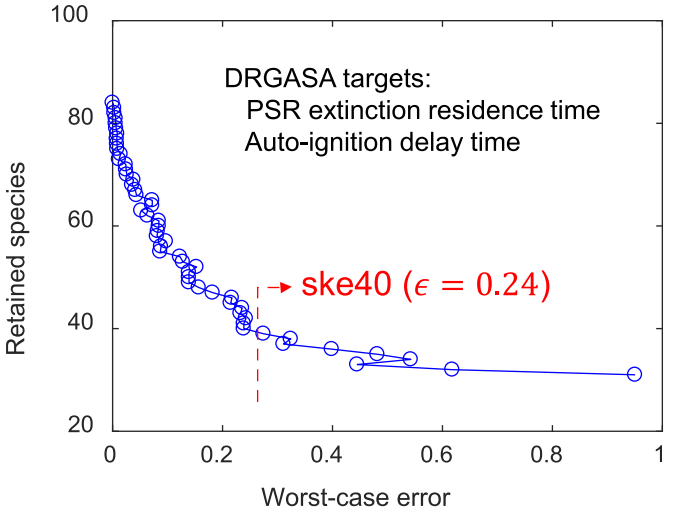

Fig. 13. Number of retained species as a function of the user-specified relative error tolerance in DRGASA.

Laminar flame speed of JP10/air at 1 atm and unburned gas temperature of 403 K is shown in Fig. 10. Data for comparison include error bars of $\pm 2\sigma$. The model prediction agrees with the experimental data within their uncertainty bounds across all equivalence ratios. Extinction strain rate comparison is also provided in Fig. 10. The model prediction agrees with data at intermediate fuel/N_2 ratio but has a larger slope with respect to the fuel to N_2 mass ratio. It was shown previously that the diffusivity of the fuel exerts a large influence on the extinction strain rate of counterflow non-premixed flames under conditions comparable to those of the current study [36]. Additional sensitivity analysis has been presented in the HyChem model development for petroleum derived jet fuels [2] also under similar conditions. Considering that the transport properties of JP10 were only estimated, the agreement is acceptable. Tests of the HyChem model against a set of non-premixed flame extinction data of Seshadri and coworkers [9] were also made and discussed in Section S3 of the SPM.

Comparisons of the high-pressure flame speed are shown in Fig. 11 at two equivalence ratios. In these two series of experiments carried out in a spherical chamber, both the unburned gas temperature and pressure rise are the result of gas compression. At higher pressures, the model underpredicts the data by <9%. The ranked sensitivity spectrum, as shown in Fig. 12, does not suggest the discrepancy to be attributable to fuel specific reactions. Rather, uncertainties in USC Mech II appear to be the leading cause for observed experiment-model discrepancies. Notably, the impact of uncertain collision efficiencies of helium in third-body reactions has already been discussed in [2].

It should be noted that even though the flame speeds show appreciable sensitivity to the key heat release reaction CO+OH=CO_2+H, the underprediction is not directly related to the CO underprediction in flow reactors. In the test model discussed in Section S2 in the SPM, CO and C_2H_2 production were boosted by the additional foundational reaction paths, but flame speed predictions only changed by approximately 1%, which is not enough to resolve the discrepancies or comparable to the prediction uncertainty caused by the foundational chemistry.

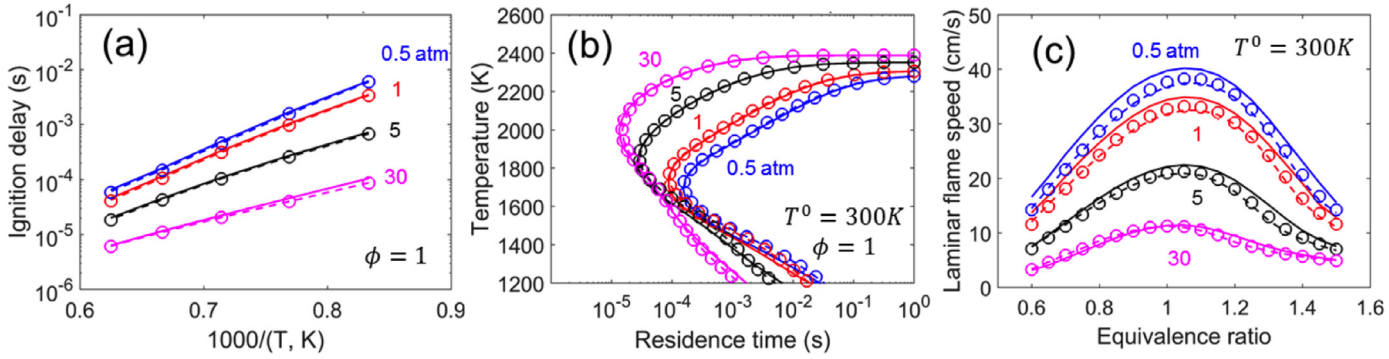

Fig. 14. Validation of the skeletal and reduced models for (a) ignition delay, (b) PSR extinction, and (c) laminar flame speed with free stream temperature of 300 K for JP10/air. Detailed: solid lines, skeletal: dotted lines, reduced: symbols.

4.3. Model reduction

HyChem model with 120 species is systematically reduced to obtain compact models that are computationally efficient for large-scale flame simulations. The reduction is based on reaction states sampled from auto-ignition and perfectly stirred reactors (PSR) covering the pressure range of 0.5–30 atm, equivalence ratio of 0.5–1.5, inlet temperature of 300 K for PSR, and initial temperature of 1000–1600 K for auto-ignition. Reduced models derived from auto-ignition and PSR have been found applicable for both compression ignition problems and flame propagation and extinction problems [37].

A skeletal model consists of a subset of species and reactions from the detailed model. The method of directed relation graph (DRG) [38] and DRG-aided sensitivity analysis (DRGASA) [39] are employed for the skeletal reduction. DRG first maps the species couplings to a graph. The species important to selected starting species are then identified through a recursive graph search. DRG is a linear time reduction method and is suitable to be applied as the first reduction step. Hydrogen atom is selected as the starting species in the present study and a threshold error tolerance of 0.3 is used to control the worst-case reduction error in both temperature and species profiles, resulting in an 85-species skeletal model. DRGASA is performed next with ignition delay and PSR extinction residence time as target parameters. DRGASA ensures the minimal skeletal model for the specified error tolerance while it is substantially more computationally expensive than DRG, and thus it is applied as the last step in the skeletal reduction. Figure 13 shows the reduction curve of DRGASA. It is seen that the number of species in the skeletal model decreases rapidly for error tolerances smaller than about 0.24 and becomes rather flat for larger error tolerances. A 40-species skeletal model is thereby obtained using DRGASA with an error threshold of 0.24.

The skeletal model is further reduced using the linearized quasi-steady-state approximation (LQSSA). Using the same reaction states sampled for the skeletal reduction, 9 species are identified as globally valid quasi-steady-state (QSS) species using a method based on computational singular perturbation (CSP) [40], and the final reduced model consists of 31 species. The QSS species are removed from the transport equations with their concentrations being analytically solved using internal algebraic equations [41].

Figure 14 shows selected validation results for the skeletal and reduced models against the detailed model for ignition delay, PSR extinction, and laminar flame speed. The worst-case error is approximately 23% for ignition delay, 28% for PSR extinction residence time, and 3.5 cm/s for flame speed. Similar agreement is observed for lean and rich mixtures ($\phi = 0.5$–1.5) for ignition delay and PSR extinction as shown in Figs. S5–S7 of the SPM along with extended validation results of counterflow extinction of premixed and non-premixed flames. Both the skeletal and reduced models are provided online at http://web.stanford.edu/group/haiwanglab/HyChem/Index.html.

5. Conclusion

Hybrid Chemistry (HyChem) approach proposed earlier for conventional, multicomponent jet fuels was tested for the single-component JP10. The HyChem model combines an experimentally derived, lumped pyrolysis model of JP10 with a detailed foundational fuel chemistry model (USC mech II). Special attention has been paid to the fuel-specific decomposition intermediates with guidance from flow reactor speciation. For JP10, cyclopentadiene must be considered as one of the key intermediates due to the 5-member ring structure in the parent exo-tetrahydrodicyclopentadiene molecule. The HyChem model gives predictions that generally agree well with experimental data, from shock tube ignition delay to laminar flame speed and non-premixed flame extinction strain rates. The exceptions are CO and C_2H_2 under flow reactor conditions where the model predicts generally lower concentrations for these species than the measurement. The global combustion property predictions are not notably impacted, even though the decomposition of JP10 is slower than other fuels tested thus far, and thus challenges some of the key assumptions of the HyChem approach. The findings herein support the applicability of the HyChem approach to single-component fuels as well.

Acknowledgment

This research was funded by the Air Force Office of Scientific Research under grant numbers FA9550-14-1-0235 (CTB, RKH and HW), FA9550-16-1-0195 (CTB, RKH and HW), FA9550-15-1-0409 (FNE), FA9550-15-1-0496 (TL), and FA9550-16-1-0079 (KB). The significant technical involvement by the AFOSR program manager, Dr. Chiping Li, is acknowledged.

Supplementary materials

The SPM contain instructions for downloading the reaction models (section S0), list of model optimization targets (section S1), additional discussion about the discrepancies CO and C_2H_2 between the flow reactor experiments and model predictions (section S2), comparisons and discussion of the HyChem model with the additional flame extinction data (section S3), and additional test results for the skeletal and reduced models.

Reaction models, including the skeletal and reduced models, can be downloaded from https://web.stanford.edu/group/haiwanglab/HyChem/Index.html

Supplementary material associated with this article can be found, in the online version, at doi:10.1016/j.combustflame.2018.08.022.

References

[1] H. Wang, R. Xu, K. Wang, C.T. Bowman, R.K. Hanson, D.F. Davidson, K. Brezinsky, F.N. Egolfopoulos, A physics-based approach to modeling real-fuel combustion chemistry - I. Evidence from experiments, and thermodynamic, chemical kinetic and statistical considerations, Combust. Flame 193 (2018) 502–519.

[2] R. Xu, K. Wang, S. Banerjee, J. Shao, T. Parise, Y. Zhu, S. Wang, A. Movaghar, D.J. Lee, R. Zhao, X. Han, Y. Gao, T. Lu, K. Brezinsky, F.N. Egolfopoulos, D.F. Davidson, R.K. Hanson, C.T. Bowman, H. Wang, A physics-based approach to modeling real-fuel combustion chemistry - II. Reaction kinetic models of jet and rocket fuels, Combust. Flame 193 (2018) 520–537.

[3] R. Xu, H. Wang, Principle of large component number in multicomponent fuel combustion - a Monte Carlo study, Proc. Combust. Inst. 37 (2018) in press, doi:10.1016/j.proci.2018.06.187.

[4] D.F. Davidson, D.C. Horning, M.A. Oehlschlaeger, R.K. Hanson, The decomposition products of JP-10, 37th Joint Propulsion Conference and Exhibit (2001) AIAA-01-3707.

[5] S.C. Li, B. Varatharajan, F.A. Williams, Chemistry of JP-10 Ignition, AIAA J. 39 (2001) 2351–2356.

[6] K. Chenoweth, A.C. Van Duin, S. Dasgupta, W.A. Goddard III, Initiation mechanisms and kinetics of pyrolysis and combustion of JP-10 hydrocarbon jet fuel, J. Phys. Chem. A 113 (2009) 1740–1746.

[7] C.W. Gao, A.G. Vandeputte, N.W. Yee, W.H. Green, R.E. Bonomi, G.R. Magoon, H.-W. Wong, O.O. Oluwole, D.K. Lewis, N.M. Vandewiele, K.M. Van Geem, JP-10 combustion studied with shock tube experiments and modeled with automatic reaction mechanism generation, Combust. Flame 162 (2015) 3115–3129.

[8] H. Li, G. Liu, R. Jiang, L. Wang, X. Zhang, Experimental and kinetic modeling study of exo-TCD pyrolysis under low pressure, Combust. Flame 162 (2015) 2177–2190.

[9] R. Seiser, U. Niemann, K. Seshadri, Experimental study of combustion of n-decane and JP-10 in non-premixed flows, Proc. Combust. Inst. 33 (2011) 1045–1052.

[10] D.A. Sheen, H. Wang, The method of uncertainty quantification and minimization using polynomial chaos expansions, Combust. Flame 158 (2011) 2358–2374.

[11] D.A. Sheen, H. Wang, Combustion kinetic modeling using multispecies time histories in shock-tube oxidation of heptane, Combust. Flame 158 (2011) 645–656.

[12] D.A. Sheen, X. You, H. Wang, T. Løvås, Spectral uncertainty quantification, propagation and optimization of a detailed kinetic model for ethylene combustion, Proc. Combust. Inst. 32 (2009) 535–542.

[13] D.F. Davidson, Y. Zhu, J. Shao, R.K. Hanson, Ignition delay time correlations for distillate fuels, Fuel 187 (2017) 26–32.

[14] T. Parise, D.F. Davidson, R.K. Hanson, Shock tube/laser absorption measurements of the pyrolysis of a bimodal test fuel, Proc. Combust. Inst. 36 (2017) 281–288.

[15] A. Fridlyand, K. Brezinsky, A. Mandelbaum, n-Heptane pyrolysis and oxidation in ethylene-methane and iso-octane mixtures, J. Propuls. Power 29 (2013) 732–743.

[16] W. Tang, K. Brezinsky, Chemical kinetic simulations behind reflected shock waves, Int. J. Chem. Kinet. 38 (2006) 75–97.

[17] S. Banerjee, R. Tangko, D.A. Sheen, H. Wang, C.T. Bowman, An experimental and kinetic modeling study of n-dodecane pyrolysis and oxidation, Combust. Flame 163 (2016) 12–30.

[18] Y.L. Wang, A.T. Holley, C. Ji, F.N. Egolfopoulos, T.T. Tsotsis, H.J. Curran, Propagation and extinction of premixed dimethyl-ether/air flames, Proc. Combust. Inst. 32 (2009) 1035–1042.

[19] C. Xiouris, T. Ye, J. Jayachandran, F.N. Egolfopoulos, Laminar flame speeds under engine-relevant conditions: uncertainty quantification and minimization in spherically expanding flame experiments, Combust. Flame 163 (2016) 270–283.

[20] H. Wang, X. You, A.V. Joshi, S.G. Davis, A. Laskin, F. Egolfopoulos, C.K. Law, USC Mech Version II. High-Temperature Combustion Reaction Model of H2/CO/C1-C4 Compounds. http://ignis.usc.edu/USC_Mech_II.htm.

[21] E. Goos, A. Burcat, B. Ruscic, Extended third millennium ideal gas and condensed phase thermochemical database for combustion with updates from active thermochemical tables. http://garfield.chem.elte.hu/Burcat/THERM.DAT.

[22] H. Wang, M. Frenklach, Transport properties of polycyclic aromatic hydrocarbons for flame modeling, Combust. Flame 96 (1994) 163–170.

[23] P. Paul, J. Warnatz, A re-evaluation of the means used to calculate transport properties of reacting flows, Symp. (Int.) Combust. 27 (1998) 495–504.

[24] L. Beneventi, P. Casavecchia, G.G. Volpi, High-resolution total differential cross sections for scattering of helium by O_2, N_2, and NO, J. Chem. Phys. 85 (1986) 7011–7029.

[25] G.P. Smith, Y. Tao, H. Wang, Foundational Fuel Chemistry Model Version 1.0 (FFCM-1). https://web.stanford.edu/group/haiwanglab/FFCM1/pages/transport.html.

[26] R.J. Kee, G. Dixon-Lewis, J. Warnatz, M.E. Coltrin, J.A. Miller, A Fortran Computer Code Package for the Evaluation of Gas-Phase, Multicomponent Transport Properties, Sandia Report SAND86-8246, Sandia National Laboratories Livermore, CA, 1986.

[27] E. Pollak, P. Pechukas, Symmetry numbers, not statistical factors, should be used in absolute rate theory and in Broensted relations, J. Am. Chem. Soc. 100 (1978) 2984–2991.

[28] H. Wang, E. Dames, B. Sirjean, D.A. Sheen, R. Tangko, A. Violi, J.Y.W. Lai, F.N. Egolfopoulos, D.F. Davidson, R.K. Hanson, C.T. Bowman, C.K. Law, W. Tsang, N.P. Cernansky, D.L. Miller, R.P. Lindstedt, JetSurF II: A high temperature chemical kinetic model of *n*-alkane (up to *n*-dodecane), cyclohexane, and methyl-, ethyl-, *n*-propyl and *n*-butyl-cyclohexane oxidation at high temperatures. http://web.stanford.edu/group/haiwanglab/JetSurF/JetSurF2.0/.

[29] D.F. Davidson, D.C. Horning, J.T. Herbon, R.K. Hanson, Shock tube measurements of JP-10 ignition, Proc. Combust. Inst. 28 (2000) 1687–1692.

[30] M. Frenklach, H. Wang, M.J. Rabinowitz, Optimization and analysis of large chemical kinetic mechanisms using the solution mapping method—combustion of methane, Prog. Energy Combust. Sci. 18 (1992) 47–73.

[31] R.J. Kee, F.M. Rupley, J.A. Miller, CHEMKIN: A General-Purpose, Problem-Independent, Transportable, FORTRAN Chemical Kinetics Code Package, Sandia Report SAND-89-8009, Sandia National Laboratories, Albuquerque, N.M., 1989.

[32] R.J. Kee, J.F. Grcar, M. Smooke, J. Miller, E. Meeks, PREMIX: A Fortran Program for Modeling Steady Laminar One-Dimensional Premixed Flames, Sandia Report SAND-85-8240, Sandia National Laboratories, Albuquerque, N.M., 1985.

[33] A.E. Lutz, R.J. Kee, J.F. Grcar, F.M. Rupley, OPPDIF: A Fortran Program for Computing Opposed-Flow Diffusion Flames, Sandia Report SAND-96-8243, Sandia National Laboratories, Livermore, CA, 1997.

[34] L. Zhao, T. Yang, R.I. Kaiser, T.P. Troy, B. Xu, M. Ahmed, J. Alarcon, D. Belisario-Lara, A.M. Mebel, Y. Zhang, A vacuum ultraviolet photoionization study on high-temperature decomposition of JP-10 (exo-tetrahydrodicyclopentadiene), Phys. Chem. Chem. Phys 19 (2017) 15780–15807.

[35] M.E. MacDonald, D.F. Davidson, R.K. Hanson, W.J. Pitz, M. Mehl, C.K. Westbrook, Formulation of an RP-1 pyrolysis surrogate from shock tube measurements of fuel and ethylene time histories, Fuel 103 (2013) 1051–1059.

[36] C. Liu, R. Zhao, R. Xu, F.N. Egolfopoulos, H. Wang, Binary diffusion coefficients and non-premixed flames extinction of long-chain alkanes, Proc. Combust. Inst. 36 (2017) 1523–1530.

[37] T. Lu, C.K. Law, Toward accommodating realistic fuel chemistry in large-scale computations, Prog. Energy Combust. Sci. 35 (2009) 192–215.

[38] T. Lu, C.K. Law, A directed relation graph method for mechanism reduction, Proc. Combust. Inst. 30 (2005) 1333–1341.

[39] X.L. Zheng, T.F. Lu, C.K. Law, Experimental counterflow ignition temperatures and reaction mechanisms of 1,3-butadiene, Proc. Combust. Inst. 31 (2007) 367-375.

[40] T. Lu, C.K. Law, A criterion based on computational singular perturbation for the identification of quasi steady state species: a reduced mechanism for methane oxidation with NO chemistry, Combust. Flame 154 (2008) 761–774.

[41] T. Lu, C.K. Law, Systematic approach to obtain analytic solutions of quasi steady state species in reduced mechanisms, J. Phys. Chem. A 110 (2006) 13202–13208.